Bioinspired catechol-based photocurable tissue sealants

Materials Today Chemistry 54 (2026) 103634

Contents lists available at ScienceDirect

Materials Today Chemistry

journal homepage: www.journals.elsevier.com/materials-today-chemistry/

Bioinspired catechol-based photocurable tissue sealants

Alba López-Moral [a,b], Miguel Ángel Moreno-Villaécija [a], Salvio Suárez-García [a], Jose Bolaños-Cardet [a], Josep Sedó-Vegara [a], Ramon Alibés [b], Juan Mancebo-Aracil [c], Haritz Sardon [d], Haeshin Lee [e], Claudio Roscini [a], Marco Sangermano [f], Félix Busqué [b,*], Daniel Ruiz-Molina [a,**]

[a] Catalan Institute of Nanoscience and Nanotechnology (ICN2), CSIC and BIST, 08193, Bellaterra, Spain
[b] Departament de Química, Universitat Autònoma de Barcelona, Bellaterra, Barcelona, 08193, Spain
[c] Instituto de Química del Sur (INQUISUR-CONICET) – NANOSYN, Departamento de Química, Universidad Nacional del Sur (UNS), Avenida Alem 1253, 8000, Bahía Blanca, Buenos Aires, Argentina
[d] POLYMAT and Department of Polymers and Advanced Materials: Physics, Chemistry and Technology, Faculty of Chemistry, University of the Basque Country UPV/EHU, Donostia-San Sebastián, 20018, Spain
[e] Department of Chemistry, Korea Advanced Institute of Science and Technology (KAIST), 291, Daehak-ro, Yuseong-gu, Daejeon, 34141, Republic of Korea
[f] Dipartimento di Scienza Applicata e Tecnologia, Politecnico di Torino, Torino, 10129, Italy

ARTICLE INFO

Keywords:
Bioinspired
Phenol
Surgical sealant
Photopolymerization
Thiol-ene

ABSTRACT

Herein we report a photocurable tissue sealant obtained through thiol-ene reaction of thiol-functionalized catechol monomers, synthesized through thia-Michael addition, with two polyethylene glycol diacrylate (PEGDA) commercial monomers in the presence of photoinitiator (PI) BAPO. The mixture is directly applied to the tissue and irradiated with both UV light and visible light (blue LED). The adhesion was studied through burst pressure (BP) measurements. Characterizations revealed very fast adhesions for gastrointestinal and external skin tissues (11.3 and 29.6 kPa, respectively), competitive with commercial products. Importantly, *in vitro* cytotoxicity confirmed the sealant biocompatibility in two cell lines (HaCaT and HFF-1) in two different assays, one incubating a piece of the cured material, and the second one curing the formulation over the cells, hence testing the biocompatibility of the procedure.

1. Introduction

Traditional clinical solutions such as sutures, clips, and staples, while reliable, often lead to complications like infections, leakage, and extended healing periods [1]. To overcome these drawbacks, innovative surgical sealants are already commercially available, being classified on natural and synthetic formulations. Most broadly used natural polymeric approaches are fibrin-based materials, with variable adhesion performance and possibility to induce allergic reactions [2], or gelatin and collagen, which even though may improve fibrin glue performance, still need to be improved for suture-free wound closing. Synthetic polymers, such as cyanoacrylates [3,4] improve adhesion performance but may exhibit higher cytotoxicity. Alternatively, PEG-based formulations exhibit greater biocompatibility but their high swelling ratios can generate high tissue stress, potentially leading to detachment [5,6]. Additional examples have been reported in the literature. Among them, pristine silk fibroin for vascular tissue healing, combined with gelatin methacrylate (GMA) for cornea perforation treatment [7] or DNA for intestine [8], crosslinked hyaluronic acid with acylates to heal dura mater [9], and recently, an *in situ* photocurable hydrogel based on diazirine-conjugated chitosan in heart aorta [10]. All in all, even though successful examples are already available, there is still a significant demand for biodegradable and/or biocompatible innovative tissue adhesives that create strong and flexible seals under humid environments while reducing curing time to decrease surgery complications.

Light-curable tissue sealants represent a particularly promising alternative due to their ability to undergo rapid and spatially controlled polymerization, typically under mild physiological conditions [11–13]. This on-demand activation enables precise application and minimizes off-target curing, making them well-suited for delicate or minimally

* Corresponding author.
** Corresponding author.
E-mail addresses: felix.busque@uab.es (F. Busqué), dani.ruiz@icn2.cat (D. Ruiz-Molina).

https://doi.org/10.1016/j.mtchem.2026.103634
Received 11 January 2026; Received in revised form 31 March 2026; Accepted 17 April 2026
Available online 26 April 2026

invasive surgical environments. Despite these advantages, many existing light-curable systems exhibit poor adhesion to wet or dynamic tissue surfaces, limiting their clinical utility. So, to enhance adhesive performance under such conditions, increasing attention has been directed toward catechol-functionalized polymers [14–16]. This field takes inspiration from the strong and durable underwater adhesion of mussels promoted by their mussel foot proteins (Mfps). This family of proteins are particularly rich in the amino acid 3,4-dihydroxyphenylalanine (DOPA), which facilitates both strong adhesions to surfaces through the formation of strong hydrogen and coordination bonds. Beyond adhesion, DOPA also facilitates cohesion through oxidative cross-linking with other catechol or organic functional groups [17,18]. All-in-all, mussel-inspired adhesives are being developed for surgical applications, offering biocompatible materials for tissue engineering [19]. Moreover, these compounds exhibit strong antibacterial properties and robust, flexible seals that are ideal for surgical applications [20].

So far, different examples have been reported. For instance, in 2022 a photocurable injectable hydrogel composed of gelatin methacryloyl catechol and PEGDA was reported to show adhesion on *ex vivo* lung models [21]; the same research group also described a photo-crosslinkable complex composite sealant for tissues, though with curing times of several minutes [22]. A little later in 2023, a light-induced crosslinking over a catechol-grafted hyaluronic acid hydrogel was shown to be effective for the sealing of gastric perforations in rats, though with modest values of adhesion strength between porcine stomach pieces [23]. The same year, an injectable complex adhesive hydrogel consisting of catechol-branched polyacrylamide network and carboxymethyl chitosan-aldehyde hyaluronic acid covalent network, showed rapid wound closure with robust mechanical strength [24]. In 2024, a hydrogel composed of a poloxamer diacrylate (poloxamer F127) and dopamine-modified hyaluronic acid methacrylate, was reported for cornea repair [25].

In spite these pioneering examples, there is a need to find novel approaches for the development of effective catechol-based light curable sealants. For this, herein we propose the synthesis of catechol-containing thiolated monomers for the obtaining of cross-linkable surgical sealants through a photocurable thiol-ene reaction. The synthesis of the monomers was already reported for strong surface adhesion (not tested in biological tissues) [26], colorless coatings for surface wettability control and give biocompatibility and colloidal stability to nanoparticles [27]. This approach, however, has never been leveraged in an active, light-triggered manner for application in tissue sealants. The schematic synthetic representation, evaluation through burst pressure (BP) measurements and its potential use, are represented in Fig. 1a.

Rooted in the efficient step-growth reaction between thiol and alkene functional groups, this chemistry offers several advantages over traditional free-radical polymerization, including rapid curing under mild conditions, low oxygen inhibition, and highly uniform network formation due to its click-like reaction mechanism [28–30]. More precisely, we propose the copolymerization of monomers **m1** and **m2** and catechol-protected monomers **b1** and **b2** with PEG-diacrylates (PEGDA) (Fig. 1b), through photoinduced thiol-ene reaction between thiol and acrylate moieties. PEG molecular weight strongly influences the mechanical and adhesive properties of PEG-based biomaterials. Increasing PEG chain length can enhance polymer network flexibility and cohesion, allowing the tuning of adhesion and mechanical performance in hydrogel systems. In this study, two liquid PEGDA - with MW 250 and MW 700 containing approximately 2 and 12 ethylene glycol units, respectively-were selected to evaluate the effect of chain length while maintaining a liquid state that facilitates formulation blending, as higher-molecular-weight PEGs tend to become semi-solid or waxy. Finally, and to validate our approach, two additional model reactions will be performed: i) the homo-polymerization of monomer **1**, and ii) the copolymerization of monomer **1** with PEG linkers without irradiation or using alternative chemical polymerization reactions and crosslinkers.

2. Materials and methods

2.1. Materials

All commercially available reagents were purchased from Sigma Aldrich except trifluoroacetic acid which was purchased on TCI. All them were used as received unless specified otherwise. Synthesis-grade solvents were purchased from Scharlab, S. L. and used without further purification. Dry Toluene was dried by distillation over the appropriate drying agent (Na^0). The synthesis of all monomers was monitored by analytical thin-layer chromatography (TLC) using silica gel 60 F254 precoated aluminium plates (0.25 mm thickness). Development was made using an UV lamp (model UVP UVGL-25) at 254 nm and using Vanillin solution. Flash column chromatography was performed using silica gel (230 - 400 mesh).

2.2. Synthesis of the monomers

*Synthesis of **m1***. To a stirred solution of sodium periodate (1.45 g, 6.80 mmol) in water (224 mL) at 0 °C, a solution of pyrocatechol (700 mg, 6.36 mmol) in diethyl ether (15 mL) was added. The solution was stirred for 5 min and then the quinone was extracted from the aqueous phase with DCM (5x 100 mL). The organic phase was dried over anhydrous sodium sulphate and filtered. In parallel, to a solution of purified trimethylolpropane tris(3-mercaptopropionate) (tristhiol from now on) (2.79 g, 7.00 mmol) in DCM (115 mL), TFA (1.46 mL, 6.80 mmol) was added. The previous organic phase with the quinone was added and stirred in the dark for 6 h. Then, the solvent was removed under reduced pressure, and the final oil was purified through flash column chromatography using a mixture of hexane and EtAcO (7 to 3) as eluent. The resulting oil was then treated with PBu_3 (111 μL, 1.10 mmol) in THF (100 mL). After 30 min, H_2O (100 mL) was added, and the mixture was stirred for an additional 30 min. Then, the volatiles were removed under reduced pressure. The resulting oil was purified by flash column chromatography with the same eluent to afford the final product **m1** in 39% yield (1.26 g, 2.49 mmol), whose spectroscopic data matched with the previously published [31,32].

*Synthesis of **m2***. It was prepared following the same protocol as for **m1**. The quinone was prepared in the same amounts, but the quantity of the thiolated monomer (pentaerythritol tetrakis(3-mercaptopropionate), tetrakis from now on) was increased to maintain the same molar proportion as the quinone (3.42 g, 7 mmol). In consequence and due to solubility issues, the crude was dissolved in higher amounts of THF and H_2O (135 mL of each solvent). The resulting monomer **m2** was obtained in 29 % yield (1.07 g, 1.56 mmol), whose spectroscopic data matched with the previously published [31,32].

*Synthesis of **b1***. To a stirred solution of purified tristhiol (5.00 g, 12.5 mmol) in dry toluene (125 mL), 3,4-dimethoxystyrene (DMS, 1.9 mL, 12.7 mmol) and 3,4-dimethoxystyrene and azobisisobutyronitrile (AIBN, 206 mg, 1.25 mmol) were added. The mixture was heated until reflux temperature and stirred under N_2 atmosphere for 4 h. Then, the crude was cooled down until room temperature, and the solvent was removed. The resulting oil was dissolved in THF (180 mL) and PBu_3 (200 μL, 1.97 mmol) was added. The mixture was stirred for 30 min. Then, water (180 mL) was added, and the mixture was stirred for additional 30 min. Then, the solvents were removed under reduced pressure to obtain a yellowish oil, which was purified by flash column chromatography using a mixture of hexane and EtAcO (7 to 3) mixture as eluent to afford the final product **b1** in 37% yield (2.62 g, 4.66 mmol). **^{1}H NMR** (300 MHz, $CDCl_3$): δ 6.84-6.71 (m, 3H, H-1, H-4, H-6), 4.07 (s, 4H, H-14′), 4.06 (s, 2H, H-14), 3.88 (s, 3H, H-7 or H-8), 3.86 (s, 3H, H-7 or H-8), 2.88 – 2.58 (m, 16H, H-9, H-10, H-11, H-12), 1.62 (t, $J_{16,11}$ = 8.1 Hz, 2H, H-16), 1.50 (q, $J_{17,18}$ = 7.6 Hz, 2H, H-17), 0.90 (t, $J_{18,17}$ = 7.6 Hz, 3H, H-18). **^{13}C NMR** (75 MHz, $CDCl_3$): δ 171.2 (C-13′), 171.0 (C-13), 149.6 (C-2), 148.4 (C-3), 147.9 (C-5), 120.6 (C-6), 112.8 (C-1), 111.0 (C-4), 62.3 (C-14, C-14′), 55.9 (C-7 or C-8), 55.8 (C-7 or C-8), 40.2

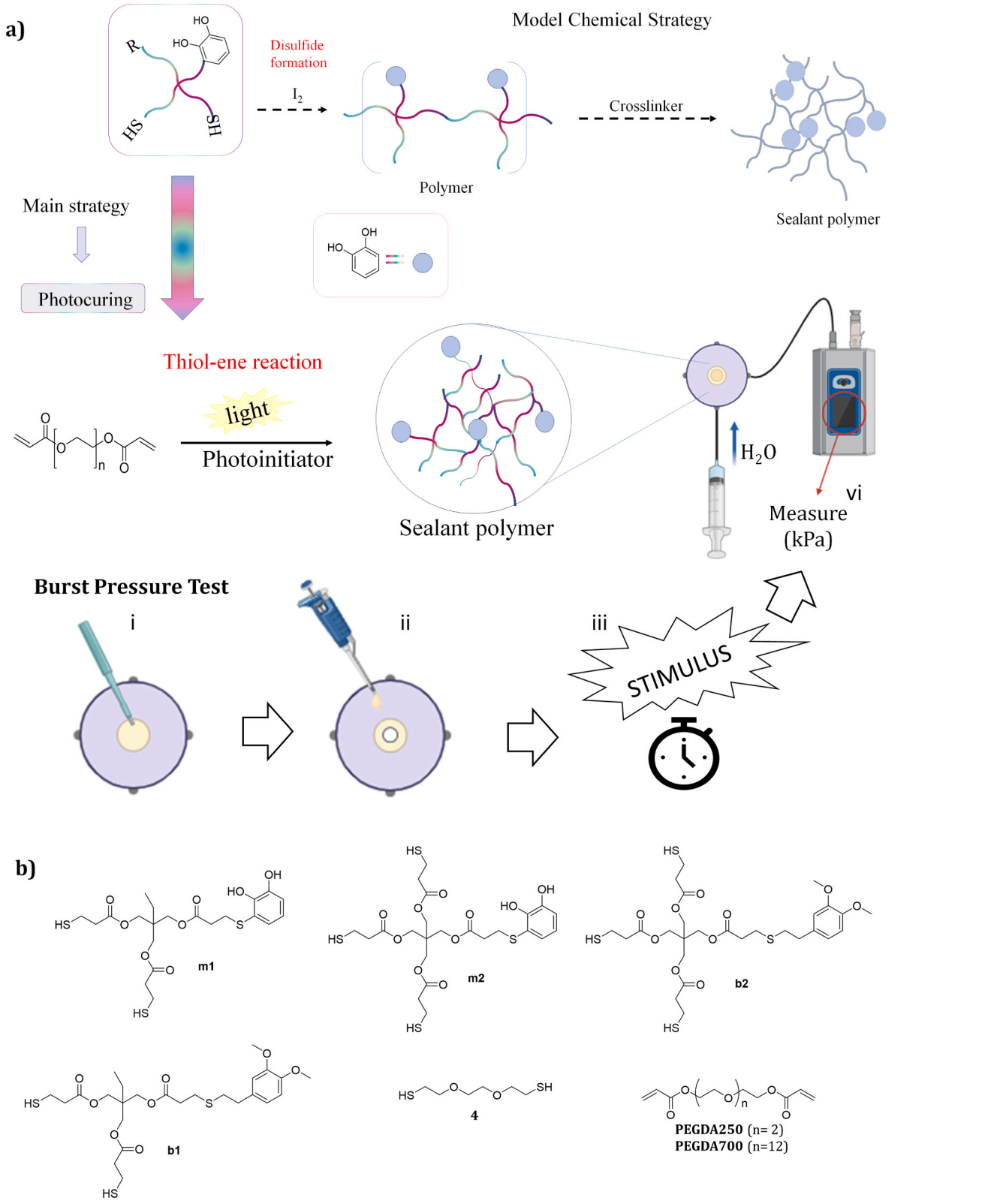

Fig. 1. a) Main strategy for the obtention of new surgical sealants and the evaluation procedure through BP measurements, which consists of: i) hole the tissue, ii) cover it with the sealant, iii) polymerize/crosslink the sealant under irradiation, and iv) measure the pressure while introducing PBS solution. b) Chemical structure of the monomers and linkers used for the sealant formulations.

(C-15), 38.5 (C-12), 36.1 (C-12′), 34.6 (C-10), 34.1 (C-9), 27.1 (C-11'), 13.2 (C-16), 19.6 (C-11), 8.9 (C-17).

Synthesis of ***b2***. It was prepared following the same protocol than for **b1** but adapting the quantity of the DMS (1.53 mL, 10.3 mmol) and AIBN (168 mg, 1.02 mmol) to maintain the molar proportion with the thiolated monomer tetrakis. The resulting monomer **b2** was obtained in 40 % yield (2.31 g, 4.10 mmol). **^{1}H NMR** (300 MHz, $CDCl_3$): δ 6.84-6.71 (m, 3H, H-1, H-4, H-6), 4.24 (m, 8H, H-14, H-14′), 3.88 (s, 6H, H-7 O H-8), 3.86 (s, 3H, H-7 O H-8), 2.96 – 2.52 (m, 20H, H-11, H-12, H-11′, H-12′, H-10, H-9), 1.63 (t, $J = 8.1$ Hz, 3H, H-16). **^{13}C NMR** (75 MHz, $CDCl_3$): δ 171.2 (C-13′), 171.0 (C-13), 149.6 (C-2), 148.4 (C-3), 147.9 (C-5), 120.6 (C-6), 112.8 (C-1), 111.0 (C-4), 62.3 (C-14, C-14′), 55.9 (C-7 or C-8), 55.8 (C-7 or C-8), 40.2 (C-15), 38.5 (C-12), 36.1 (C-12′), 34.6 (C-10), 34.1 (C-9), 27.1 (C-11'), 19.6 (C-11).

2.3. Synthesis of polymeric materials

Synthesis of ***p1***. **m1** (506 mg, 1.0 mmol) and $NaHCO_3$ (134.4 mg, 1.6 mmol) were mixed in EtOH 96 % (0.5 mL). Then, a solution of iodine (190.5 mg, 0.75 mmol) dissolved in EtOH 96% (1.5 mL) was added over the previous one at 300 μL/min with a syringe pump. Once added, the reaction was left under magnetic stirring at 800 rpm for 20 min at room temperature. The final mixture was dried under reduced pressure. The oligomeric fraction was isolated by extracting the crude material in DCM:H_2O to remove the excess of salts. The organic phase was collected, dried with anhydrous Na_2SO_4 and filtered. The final material **p1** was obtained after drying the solvent under reduced pressure for 48 h affording a colorless viscous liquid (412 mg).

Synthesis of p(1-4). **m1** (253 mg, 0.5 mmol), dithiol **4** (81.4 μL, 0.5 mmol) and sodium bicarbonate (147.0 mg, 1.75 mmol) were mixed in EtOH 96% (500 μL). Then, a solution of iodine (211.0 mg, 0.83 mmol) dissolved in EtOH 96% (1.5 mL) was added at 300 μL/min with a syringe pump. Once added, the reaction was left under magnetic stirring at 800 rpm for 20 min at room temperature. The final mixture was dried under reduced pressure. The oligomeric fraction was isolated by extracting the mixture in DCM:H_2O to remove the excess of salts. The organic phase was collected, dried with anhydrous Na_2SO_4 and filtered. The final material was obtained after drying the solvent under reduced pressure for 48 h affording a colorless viscous liquid (321 mg).

Synthesis of the sealing materials through photopolymerization. All the formulations were prepared by the same experimental procedure applying the quantities described on Table 1 using 1 equivalent of the thiol derivative and 1 equivalent of the acrylate-containing monomer. As an example, **b2** (420 mg, 0.75 mmol) and PEGDA700 (718 mg, 1.03 mmol) were mixed inside an Eppendorf vial covered with foil to avoid light contact. Then PI phenylbis(2,4,6-trimethylbenzoyl)phosphine oxide BAPO (23 mg, 0.055 mmol, 2% wt) was added and the mixture was stirred with a spatula until complete integration of the components. The resulting yellow oil was stored on the fridge in darkness until use. All the formulations were photopolymerized under UV lamp at 48 mW/cm^2 for 60 s.

2.4. Characterization

Characterization of monomers and reference polymers ***p1*** *and* ***p(1-4)***. The NMR spectra of the four monomers were recorded at Bruker Ascend 200 (300 MHz). Proton chemical shifts are reported in ppm (δ) (CDl_3, 7.26 ppm). The ^{1}H NMR spectra of the homopolimer **p1** and the copolymer **p(1–4)** were recorded at Bruker Avance III 400sb (400 MHz). Proton chemical shifts are reported in ppm (δ) (CDl_3, 7.26 ppm). Molecular weights were found by gel permeation chromatography (GPC) using an Agilent Technologies 1260 Infinity chromatograph and THF solvent. The instrument was equipped with three gel columns: PLgel 5 μm Guard/50 × 7.5 mm, PLgel 5 μm 1000 Å MW 4K–400K, and PL Mixed gel C 5 μm mw 200-3 M. Calibration was made by using PMMA STANDARDS. In each experiment, the polymer was dissolved in THF (2 mg/mL) and analyzed by GPC (1 mL/min flow; 40 °C column temperature).

Characterization of photopolymerized materials. The infrared spectra (IR) of photopolymerized polymers were recorded on a Bruker Tensor 27 Spectrophotometer equipped with a Golden Gate Single Refraction Diamond ATR (Attenuated Total Reflectance) accessory at Servei d'Anàlisi Química of the Universitat Autònoma de Barcelona. Peaks are reported in cm^{-1}.

Conversion assessment of photopolymerized formulations. The photocuring process was followed by means of a Nicolet iS50 FTIR Spectrometer. The FTIR spectrometer was equipped with a mercury lamp, Hamamatsu LIGHTINGCURE LC8 (Hamamatsu Photonics), with an optic fiber to direct irradiate the samples. The emission of UV-light was centered at 365 nm and the intensity was around 48 mW/cm^2. The formulations were spread on a silicon slice with a thickness of 12 μm by means of film bar. The spectra were collected with a spectral resolution of 4 cm^{-1}. All the data were handled by OMNIC software developed by Thermo Fisher Scientific. The conversion curves were collected by monitoring the disappearance of the thiol peaks and the carbon-carbon double bond of acrylate functionalities at 2575 cm^{-1} and 812 cm^{-1} respectively. The peak at 1730 cm^{-1} was taken as reference, corresponding to the carbonyl doble bond of acrylate moieties. It was assumed to be unaffected by UV-irradiation since this functional group is not involved in the photopolymerization process. Equation (1) is used to calculate the conversion for each functional group, where A_{fun} is the area of the peak that we are analyzing at time x and A_{ref} is the area of the reference peak.

$$Conversion\ (\%) = \left(1 - \frac{\left(A_{fun}/A_{ref}\right)_{t=x}}{\left(A_{fun}/A_{ref}\right)_{t=0}}\right) x100 \quad (1)$$

Mechanical characterization of photopolymerized polymers. The thermo-mechanical analysis of the photocured materials was carried out by dynamic mechanical thermal analysis (DMTA) with a Triton Technology instrument. The initial temperature was achieved by cooling down the test chamber with liquid nitrogen; for some samples the starting temperature was −50 °C and for others −30 °C, depending on the Tan δ profiles for each formulation. The heating rate was set at 3 °C/min. The instrument applied uniaxial tensile stress at frequency of 1 Hz.

Table 1
Quantities used to prepare all the formulations tested, where T-deriv. refers to the thiol-containing monomer corresponding to each formulation, and A-deriv. refers to the acrylate-containing PEG chain of each formulation.

Formulation	T-deriv. quantity	T-deriv. mmol	A-deriv. quantity	A-deriv. mmol	BAPO quantity	BAPO mmol
p(b2-PEGDA250)	790 mg	1.4	0.460 mg	1.84	25 mg	0.06
p(b1-PEGDA700)	450 mg	0.8	550 mg	0.79	20 mg	0.05
p(b1-PEGDA250)	560 mg	0.99	235 mg	0.94	14 mg	0.03
p(m2-PEGDA700)	346 mg	0.58	654 mg	0.93	22 mg	0.05
p(m2-PEGDA250)	600 mg	1.0	377 mg	1.5	26 mg	0.06
p(m1-PEGDA700)	400 mg	0.79	552 mg	0.79	18 mg	0.04
p(m1-PEGDA250)	446 mg	0.88	220 mg	0.88	14 mg	0.03

The measurement was done to detect the glass transition temperature (T_g) as maximum of Tan δ curve and was stopped after the rubbery plateau. The samples were UV-cured in a silicon template with average dimension of 8.3 × 18 × 0.6 mm and using a DYMAX lamp (DYMAX ECE ZIP™ shutter 5000) with 130.9 mW/cm^2 intensity, measured at 10 cm from the bottom of the lamp. Equation (2) is derived from the statistical theory of rubber elasticity and provides an approximation of the crosslinking density· where νc is the number of crosslinks per volume of the crosslinked network ($\frac{mol}{m^3}$), E' is the storage modulus in the rubbery plateau (T_g+ 50 °C, $\frac{J}{m^3}$ as units), R is the gas constant ($\frac{J}{mol \cdot K}$) and T is the temperature expressed in Kelvin.

$$\nu c \left(\frac{mol}{m^3}\right) = \frac{E'}{3RT} \quad (2)$$

In vitro physiological stability assessment of the ***p(b2-PEGDA700)*** *formulation*. Three pieces of the cured material were freeze-dried and weighed (W_0). Then, they were soaked on a PBS solution (pH 7.4) at 37.5 °C. After 30 min, the pieces were softly dried with paper and weighed (W_t). This procedure was repeated until the material didn't absorb water anymore. Then, the equilibrium swelling rate (ESR, %) was calculated with Equation (3).

$$ESR\ (\%) = \frac{W_2 - W_1}{W_1} \cdot 100 \quad (3)$$

To study the mass loss of the polymer, 12 pieces of cured material were freeze-dried, weighted, and soaked on PBS solution (pH 7.4) at 37.5 °C. The samples were freeze-dried and weighed again in groups of three after 3, 7, 10 and 14 days. The degradation ratio (%) was calculated with Equation (4) and plotted to see the evolution.

$$Degradation\ ratio\ (\%) = \frac{W_1 - W_2}{W_1} \cdot 100 \quad (4)$$

2.5. Ex vivo sealing tests

Sample preparation. All the tissues used were extracted from pigs and donated by the Veterinary School of the UAB. They were stored at −4 °C until used. Before its use, the tissues were soaked on distilled water. After 30 min, they were sliced in squared pieces of 5 cm approximately to cover all the surface of the metallic platform used for BP measurements. Then, a 3 mm hole was done in the middle with a 3 mm biopsy punch.

Burst pressure measurements. BP values were obtained following the standard methodology descripted on ASTM-F2392-04. The 3 mm hole done with a biopsy punch in the tissue was covered with 20 μL of the formulation and cured for 1 min under irradiation. The test was proceeded by increasing the pressure of the system with a syringe pump with distillate water at 17 mL/min rate until the pressure registered by the manometer went down. A minimum of 3 replicates were performed for each formulation. The syringe pump used for the experiment was a two-channel syringe pump multi-phaser™, model NE-4000 (KD technology) and the manometer was a RSO PRO Manometer RS-8890D.

2.6. In vitro biocompatibility tests

Sample preparation. The formulation was photopolymerized in a UVP Crosslinker CL-3000L (Analytik Jena US) using a handmade template (30 × 10 × 0.25 mm) composed of a perfluorinated glass base and silicon borders.

Cell culture. Human fibroblasts (HFF-1, ATCC SCRC-1041) and keratinocytes (HaCaT, ATCC PCS-200-013) were cultured in 75 cm^2 flasks (Falcon™ 353136) with 12 ml of Dulbecco's modified Eagle's medium (DMEM) supplemented with 100 μg/ml streptomycin, 100 U/ml penicillin, and 10% heat-inactivated foetal bovine serum (Invitrogen). Cultures were maintained at 37 °C in 95% air/5% CO_2 and high humidity (Fisherbrand™ Isotemp™ incubator). Cells were harvested at 80–90% confluence using 0.05% trypsin-EDTA (3 min for HFF-1; 8 min for HaCaT), neutralized with DMEM + 10% FBS, centrifuged (200 rpm, 5 min), and resuspended to the desired density. All procedures were carried out under sterile conditions in biosafety level 2 laminar flow cabinets.

Cell viability assay with the cured material. Cytotoxicity of the cured formulation was assessed by nuclear staining with Hoechst 33342 (H42) and propidium iodide (PrI). HFF-1 and HaCaT cells (0.5 × 10^5 and 1 × 10^5 cells/well, respectively) were seeded in 96-well plates (Falcon™ 353072) and incubated for 24 h. Each well then received either medium alone (control) or a UV-sterilized polymer disc (4 mm diameter, 0.25 mm height). After 24 h incubation, cells were exposed to medium containing PrI (1 μg/ml) and H42 (2 μg/ml) for 30 min at room temperature in the dark. Imaging was performed under phase contrast and fluorescence using a Nikon ECLIPSE TE2000-E microscope with Hamamatsu ORCA-ER camera. Nuclei were counted manually in ImageJ, and cell death was calculated as the percentage of PrI-positive over total H42-positive cells. Experiments were performed in eight replicates (n = 8).

Cell viability assay with in situ photopolymerization. Cytotoxicity of the material during the application was assessed by nuclear staining with H42 and PrI. HFF-1 and HaCaT cells (0.5 × 10^6 and 1 × 10^6 cells/well, respectively) were seeded in 12-well plates (Falcon™ 353043) and incubated for 24 h. Each well then received a 3 μL drop of the formulation and was irradiated for 90 s with the blue LED (λ = 430 nm) to prevent cell death due to UV irradiation. Then each well was filled with medium and incubated for 24 h. Next day images were recorded to assess the viability of the cells surrounding the material.

2.7. In vivo biocompatibility tests

Animals. All procedures were approved by the Animal Care Committee of KAIST (KA2017-44) and conducted at Knotus Co. Ltd. (Incheon, Republic of Korea). Three 18-week-old male New Zealand White rabbits (Hallim Experiment Animal, Korea) were acclimated for two weeks under controlled conditions (23 ± 3 °C, 55 ± 15% humidity, 12 h light/dark cycle, 150–300 lx, 10–20 air changes/h). Animals had ad libitum access to sterilized tap water and commercial food (Dream Bio, Korea). Fur on the dorsal area was clipped 12 h before testing.

Procedure. Prior to application, rabbits were anesthetized with a subcutaneous injection of Zoletil 50 (5 mg/kg, VIRBAC) and xylazine (2.5 mg/kg, Bayer). A volume of 200 μL of the liquid formulations **p(b2-PEGDA700)** or **p(b1-PEGDA700)** was applied at three different dorsal sites per animal. Each site was then irradiated for 60 s with a UV lamp (48 mW/cm^2) to induce *in situ* photopolymerization. Control sites received no formulation. The application areas were examined every 24 h for three consecutive days. Skin reactions (erythema, edema, or other signs of irritation) were evaluated according to the guidelines described in ISO 10993-10:2010.

Data analysis. All data were processed and plotted using *OriginPro* (OriginLab Corporation, Northampton, MA, USA). Results are expressed as mean values ± standard deviation (SD).

3. Results and discussion

3.1. Synthesis of monomers

Monomer **m1** was obtained in a 39% yield through a methodology previously described by our research group for the conjugation of thiolated derivatives with catechol moieties [31,32]. Briefly, the catechol is converted to the corresponding quinone under oxidative conditions using $NaIO_4$, extracted with dichloromethane (DCM), and directly added to a tristhiol solution to form a S–C bond through a 1,6-thia-Michael addition (Scheme 1a). Purification of monomer **m1** by column chromatography revealed the presence of disulphide-containing side products, including self-cyclization species, most of them easily

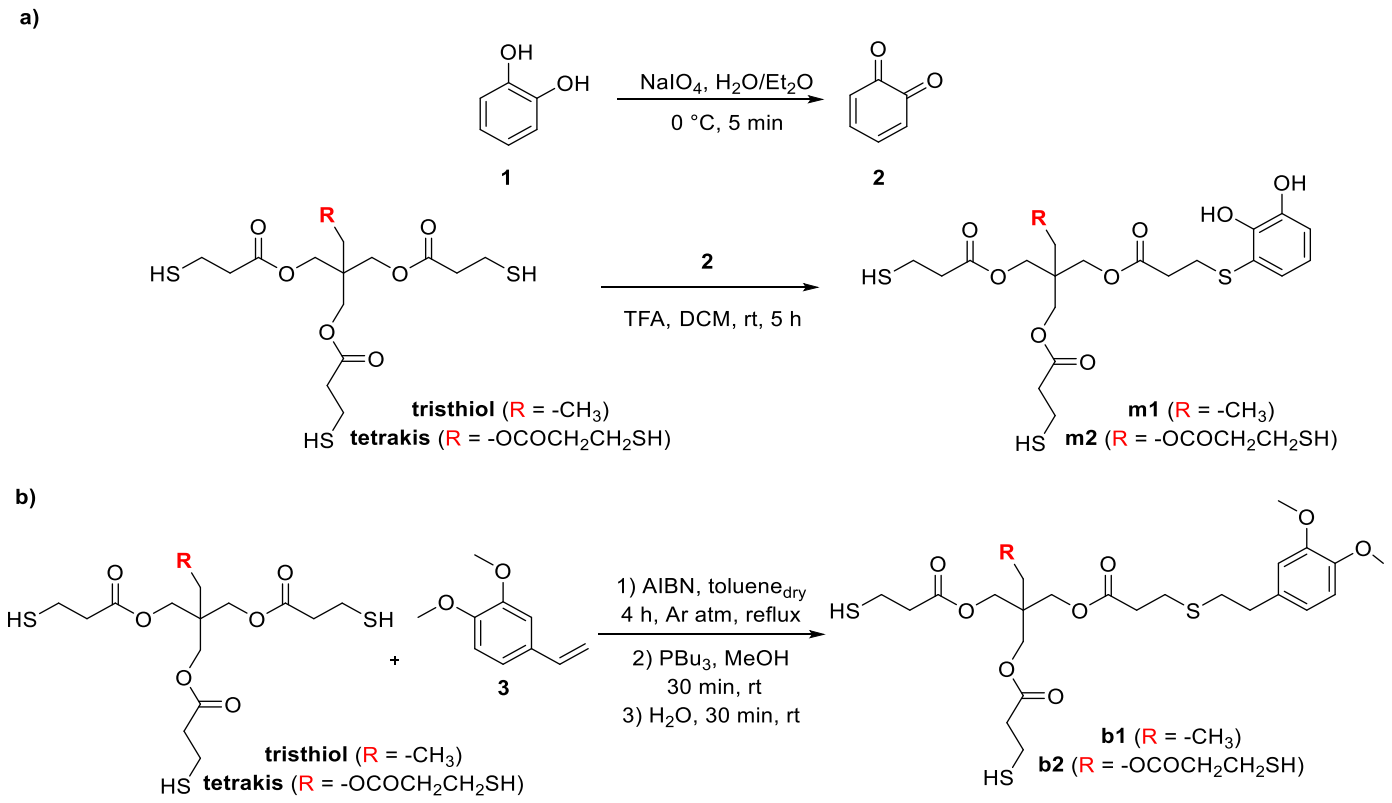

Scheme 1. Synthesis of a) monomers **m1** and **m2**, and b) monomers **b1** and **b2**.

removed. Even several conditions were evaluated, the dimerization byproduct could not be removed by column chromatography. The presence of the dimer was detected by excess integration in the ^{1}H NMR between 2.65 and 2.85 ppm, corresponding to the –CH_2CH_2- signals of both the tristhiol and its dimer. To resolve this, the crude mixture was treated with PBu_3 to reduce disulphide bonds to thiols, so converting the dimerization byproduct into the starting material tristhiol, which was easily removed from **m1** by column chromatography. Similarly, monomer **m2** was obtained in a 29% yield substituting the tristhiol by tetrakis.[29] ^{1}H NMR analysis indicated the presence of disulfide-linked byproducts, prompting analogous treatment of **m2** with PBu_3 to reduce these to the starting tetrakis, thus facilitating the purification of **m2** by column chromatography.

Monomers **b1** and **b2**, were obtained in 37% and 40% yield, respectively, through a thermally activated thiol-ene reaction between 3,4-dimethoxystyrene (DMS) and either tristhiol or tetrakis, catalyzed by AIBN (Scheme 1b) [26], as a radical initiator that decomposes upon heating into cyanoisopropyl radicals and $N_{2(g)}$, initiating the reaction by abstracting hydrogen from the thiols groups producing thiyl radicals, which in turn add to the vinyl group of DMS, generating carbon-centered radicals that propagate the reaction by abstracting hydrogen from additional thiol molecules, thereby completing the catalytic cycle of the reaction. As with the monomers **m1** and **m2**, the corresponding thiol dimers impurities were identified by ^{1}H NMR. Following the same strategy as for **m1** and **m2**, the dimers were reduced with PBu_3 and the resulting starting tristhiol or tetrakis removed through column chromatography. Notably, in this case the number of side-products obtained during the ene reaction was much lower than for catechol derivatives, allowing the PBu_3 treatment to be applied directly to the crude reaction mixture, thereby avoiding the intermediate purification step.

3.2. Photopolymerization

The polymerization of the photocrosslinkable formulations was carried out following a standardized procedure for all the reported combinations described in this work (schematic representation in Fig. 2a). Briefly, thiol-containing monomers were mixed with commercially available PEGDAs. Two lengths of PEGDA were evaluated, PEGDA250 and PEGDA700 with 2 and 12 ethylene units, respectively. A thiol-to-acrylate molar ratio of 1:1 was selected to ensure stoichiometric equivalence between reactive groups, which promotes efficient network formation and maximizes functional group conversion. The PI BAPO was added to the mixture of monomers (2% wt) [33] and the formulations were stirred until BAPO was completely dissolved and stored in an Eppendorf covered with foil to avoid light contact. The formulations were cured under a UV lamp at 48 mW/cm^2 for 1 min.T_gs and cross-linking densities (ν) were calculated from DMTA analyses. These experimental conditions were selected after much experimentation to favor complete polymerization, thus avoiding the known toxicity of unreacted acrylate groups [34] and photoinitiator byproducts [35]. As previously reported [36], this issue can be countered by adequate UV-light exposure, as demonstrated by the good results of biocompatibility obtained (vide infra).

*Photopolymerization of **m1** and **b1***. Results showed lower T_g for the formulation with PEGDA700 (−25.1 °C and −34.2 °C for **m1** and **b1**, respectively) than for the formulation with PEGDA250 (−2.6 °C and −9.95 °C for **m1** and **b1**, respectively), pointing out to the higher flexibility provided by longer PEG chains (this tendency can be appreciated in the **m1** DMTA plots of Fig. 2b). Accordingly, this flexibility is also higher for both **b1** polymers thanks to the additional styrene moiety. Considering the density of **m1** formulations, it was higher for PEGDA250 (199 mol/m^3) than for PEGDA700 (174 mol/m^3), in agreement with the shorter distances between cross-linking points for the first case. However, this tendency was not observed in **b1** formulations. In this case, poor reproducible analyses were obtained, and the cross-linking densities were 366 mol/m^3 for PEGDA700 and 18 mol/m^3 for PEGDA250, contrary to expected values.

*Photopolymerization of **m2** and **b2***. Similar tendencies were found for

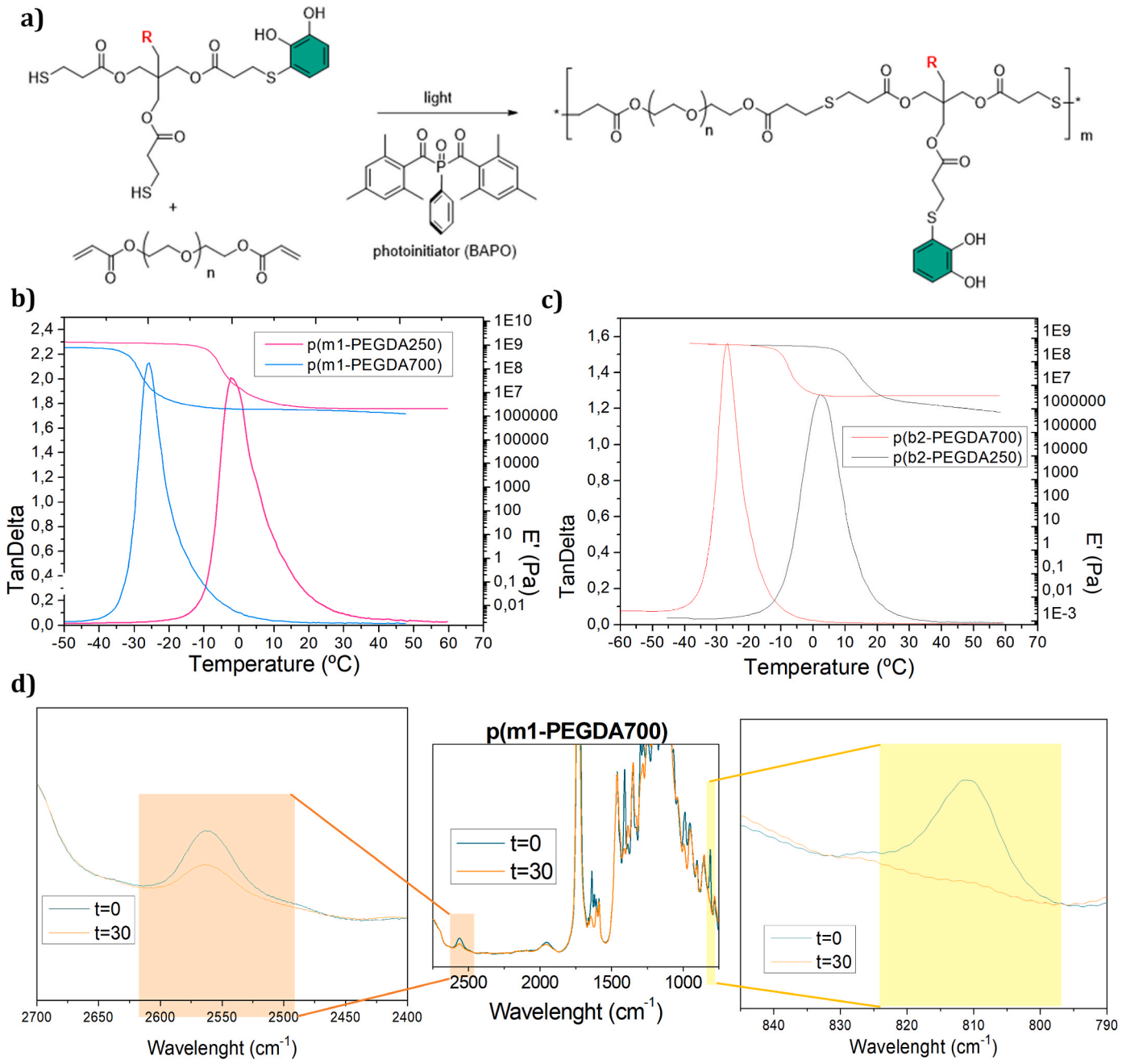

Fig. 2. a) Scheme of the photochemical reaction occurring during the curing process of the photocurable formulations. b) DMTA plots of the **p(m1-PEGDA250)** and **p(m1-PEGDA700)** (pink and blue, respectively). T_g of the PEGDA250 formulation is 30 °C higher than for PEGDA700 formulation, demonstrating that longer PEG produce more flexible materials. c) DMTA plots of **p(b2-PEGDA250)** and **p(b2-PEGDA700)** (black and red, respectively). Again, PEGDA250 displays T_g ~30 °C higher than PEGDA700 formulations. d) Analysis of the reduction of the thiol (orange) and acrylate (yellow) signals during the photopolymerization analyzed by real-time FTIR during the first 30 s of irradiation for the synthesis of **p(m1-PEGDA700)**.

m2 and **b2**. PEGDA700 formulations presented lower T_gs (−26.7 °C for **m2** and -30.9 °C for **b2**), in comparison to PEGDA250 (4.4 °C for **m2** and -2.0 °C for **b2**), associated to the higher flexibility provided by the longer PEG chains (see Fig. 2c). Concerning the density, PEGDA250 formulations displayed 228 and 291 mol/m^3 for **m2** and **b2**, respectively, while PEGDA700 formulations showed 552 and 505 mol/m^3. From here it may be possible to deduce that, as expected, cross-linking densities were higher than those for **m1** in all cases, demonstrating the influence of the extra cross-linking point provided by the new free thiol. However, when comparing the cross-linking densities among PEGDA250 and PEGDA700 formulations, PEGDA700 formulations displayed two times the cross-linking densities than their equivalents with PEGDA250. This result was unexpected according to the length of the PEG chains. To explain this behavior, real-time FTIR experiments revealed much lower conversion in PEGDA250 formulations for both acrylate and thiol moieties than in PEGDA700 formulations. Incomplete conversions in PEGDA250 formulations were attributed to kinetic and diffusional limitations associated with increasing viscosity and reduced chain mobility, which decreased the cross-linking density of the final materials [35].

3.3. Sealing studies of photopolymerized materials

The sealing ability was evaluated *ex vivo* on porcine intestine following the protocol established in ASTM F2392- 04 to test the burst

strength of surgical adhesives. The formulation of interest was placed on the porcine intestine covering completely a 3 mm hole preformed with a punch, so 30 μL of the monomer formulations were enough to cover it. Afterwards, the samples were cured with a UV lamp placed at 5 cm distance and using an intensity of 48 mW/cm^2 for 60 s. And finally, the manometer was turned on to measure in real time the hydraulic pressure that the sealant could support while the PBS solution was slowly introduced by the syringe pump. The maximum pressure supported until the sealant broke was recorded by the manometer (the setup is presented in Fig. 3a).

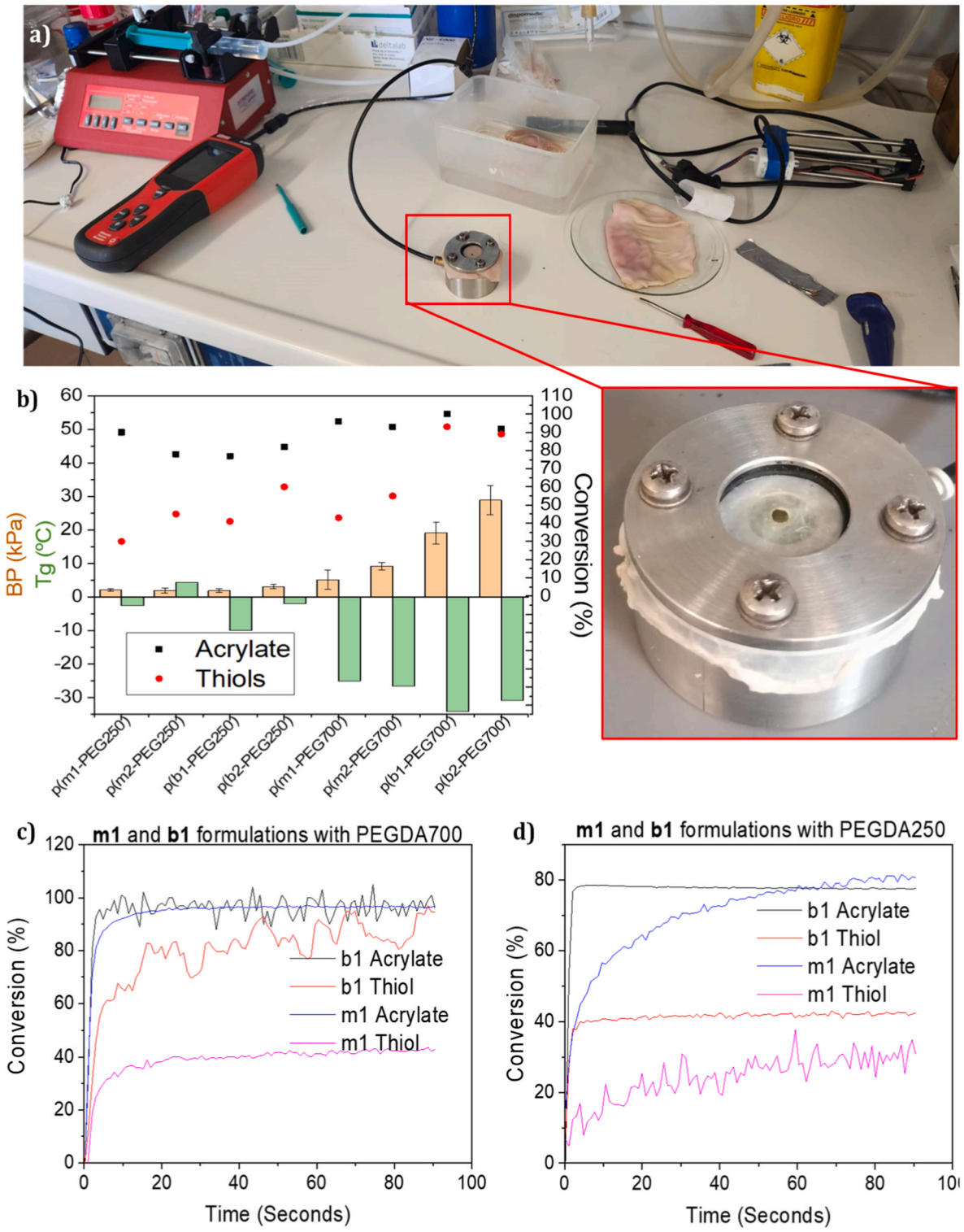

Fig. 3. a) Setup of the BP measurements during photopolymerizations. b) Glass transition temperature (T_g, green bars), BP (orange bars), and conversions of acrylates (black squares) and thiols (red dots) of the photocrosslinked materials. It demonstrates a correlation between higher conversion rates, higher burst pressures, and lower T_gs. c) Conversion of acrylates and thiols during the photopolymerization of PEGDA700 with **m1** and **b1**. The conversion of acrylates and thiols is much similar in **b1** formulations than in **m1** ones. d) Conversion of acrylates and thiols during the photopolymerization of PEGDA250 with **m1** and **b1**. The conversion rates are much lower than for PEGDA700 formulations and there is no match among thiol and acrylate conversion in any PEGDA250-based formulation.

The material resulting from the photopolymerization of **m1** and **m2** with **PEGDA250** displayed BP values of 2.1 kPa and 1.9 kPa, respectively. As expected, similar results were obtained for the blank materials **p(b1-PEGDA250)** and **p(b2-PEGDA250)**, with values of 1.9 kPa and 3.1 kPa, respectively. Better results were obtained when using PEGDA700. In this case, **p(m1-PEGDA700)** and **p(m2-PEGDA700)** yielded values of 5.1 kPa and 9.2 kPa, respectively. Unexpectedly, even much higher values were obtained for the blank materials. In this case, **p(b1-PEGDA700)** and **p(b2-PEGDA700)** yielded values of 19.1 kPa and 28.9 kPa. The unexpected worse performance of catechol-containing photocurable formulations was attributed to their strong tendency to react with radicals. Hence, catechols could act as inhibitors of the polymerization leading to lower global tiol-ene conversions. To evaluate these unpredicted results, the curing process was studied with real-time FTIR, following the thiol conversion at 2570 cm^{-1} (S–H bond) and at 812 cm^{-1} (C═C bond) for acrylate moieties (Fig. 2d). The results showed photopolymerization of blanks **b1** and **b2** yielded better conversion rates mainly for PEGDA700. Indeed, **p(b1-PEGDA700)** presented 100% and 93% conversions of acrylates and thiols while **p(b2-PEGDA700)** presented 92% and 89% conversions, which nicely align with the best BP results obtained. The lower correlation between acrylate and thiols conversions in catechol-containing formulations is appreciated in Fig. 3b, which supports the inhibition of the thiol-ene mechanism. Fig. 3b also presents the correlation between the sealant capacities (BP) and the polymerization conversions and flexibility (lower T_gs)(for exact values see Table 3 section 3.3 of the supporting information). Free thiols may play a relevant role since all the formulations with three free thiols (**m2** and **b2**) present higher BP than the corresponding dithiol derivatives (**m1** and **b1**).

To shed more light on the matter, two additional model reactions were done. The first one was the homo-polymerization of **m1** (**p1**). For this, a 3 mm diameter hole was covered with 30 μL of **p1** and measured after 5 min, resulting in a BP value of 0.3 ± 0.1 kPa. Aimed to improve this result, a 12 μL of a 0.25 M additional crosslinkers were added. The addition of iron (II) acetate solution slightly increased the BP value up to 0.5 ± 0.2 while with $NaIO_4$ increased up 1.3 kPa, which do not represent a significant increase. The second one consisted in the copolymerization of **m1** with thiolated PEG linkers using alternative chemical polymerization reactions and crosslinkers instead of light (for the synthetic optimization of both polymers see Supporting Information section 2). In the case of **p(1–4)**, a BP of 0.3 ± 0.2 kPa was obtained after 5 min curing. With iron (II) acetate no change in the BP was observed while the $NaIO_4$ solution increased the BP value up to 5.4 ± 1.2 kPa. In any case, all these values are significantly smaller than the ones obtained with the photopolymerization-based strategy.

The curing process of the formulation **p(b2-PEGDA700),** which exhibits the best sealing performance, was also studied under a less harmful 430 nm LED. The formulation took 90 s to cure (instead of 60 s) and the BP was 11.3 ± 0.94 kPa, 2.5 times lower than curing under UV light (28.1 kPa). Though, these values are still within the range of commercially adhesives, including a fast and more biocompatible curing process. For instance, using the experimental conditions previously described and used for **p(b2-PEGDA700)**, the PEG based formulation CoSeal® achieves initial gelation within 2-5 min, though it is not fully polymerized at least til 15-20 min [37]. Tisseel® (fibrin glue) sealing also takes from 2 to 5 min [38]. Concerning the BPs, Baxter™ reports that CoSeal® withstands up to 88 kPa only if combined with sutures, while Tisseel® BPs, yielded 4 kPa in gastrointestinal tissues [39], three times lower than the obtained with **p(b2-PEGDA700)** (11.3 kPa). Finally, to broaden the scope of application, **p(b2-PEGDA700)** was tested over external skin using the blue LED irradiation, reaching 29.6 ± 2.6 kPa of BP, very similar results compared with a commercial cyanoacrylate-based sealant, specifically used for external skin sealant (Dermabond®, 26 kPa) [40]. Comparing with the other noncommercial photocurable polymeric materials referred in the introduction and including catechol moieties, these results with p(b2-PEGDA700) result also competitive. Thus, burst pressure values of 20.2 ± 3.4 kPa [21], 30.1 ± 1.3 kPa [23], and 38.1 ± 7.2 kPa [25] have been described for porcine lung, stomach and cornea samples, respectively, although these studies used more complex composite materials and required curing times of several minutes. In the case of using another complex catechol-grafted hydrogel based on a non-photocurable curing mechanism, a remarkable value of 38.2 ± 4.0 kPa is obtained in porcine intestine samples, with a gelation time up to 1 min [24]. In an important precedent of photocurable diazirine-chitosan based material, not including catechol units, a notable BP value of 26.6 ± 3.5 kPa is reported using porcine heart aorta [10].

3.4. Analysis of p(b2-PEGDA700)

Stability. The swelling capacity of a surgical adhesive is directly related to the degree of degradation and the absorption of by-products in the wound environment, which in turn influences wound healing. It can induce the premature detachment of the material with the substrate or, at least, weaken the interactions. Therefore, it is interesting to evaluate the BP of the samples after reaching the ESR in biological conditions. After determining the time to reach the ESR (90 min, Fig. 4a) the BP after swelling was 11.1 ± 1.3 kPa, still demonstrating good stability after the swelling process. Moreover, the calculated ESR was 44%, well below the appropriate ESR 150% value reported in the literature for surgical sealants [41].

Degradation. Degradation studies (see Supporting Information) were carried out for 14 days. Results of Fig. 4b show a faster degradation of the samples along the first three days, with weight loss of 1.5%. From then on, a linear tendency could be observed till the end of the study (day 14). This linear behavior allowed us to calculate the rate of degradation (0.02%/day) and to predict at longer times. For instance, a ≈45% of degradation would be expected after one year of application, ensuring sealing until regeneration, as soft tissues injuries typically take from three to twelve months to fully heal (depending on the grade of the injury) [42,43].

In vitro biocompatibility. The biocompatibility tests were performed with two immortalized human cell lines: fibroblasts (HaCaT) and keratinocytes (HFF-1). fibroblasts cells are the most common cells of connective tissue in animals and play a crucial role in wound healing [44]. On the other hand, keratinocytes were selected as these cells constitute 90% of the epidermal skin cells, which is the outermost layer of skin [45]. The cytotoxicity evaluation of **p(b2-PEGDA700)** demonstrated an outstanding cell viability above 99% for both HaCaT and HFF-1 cells (Fig. 4c and e).

Cell viability studies within *in situ* polymerization are shown in Fig. 4e, where three distinct regions of cells can be differentiated. Region **A** is composed of cells which were immobilized and fixed with the sealant, maintaining their morphology. Region **B** represents the periphery of the polymerized sealant. Despite no appreciable cell death was observed (PrI Filter), slight changes in their morphology were appreciated (Bright Field). Finally, region **C** is comprised by unaffected and viable cells, where no change in morphology or signs of cell death was observed. These results support the great biocompatibility previously achieved, highlighting the potential applicability of the material for biomedical purposes.

In vivo biocompatibility. The *in vivo* biocompatibility studies were performed on New Zealand White rabbits (n = 2). A volume of 200 μL of the formulations **p(b2-PEGDA700)** and **p(b1-PEGDA700)** was applied to three dorsal sites per animal, followed by irradiation for 60 s under UV light to induce *in situ* photopolymerization. Control sites without formulation were also included. The treated areas were examined at 24, 48 and 72 h post-application (Fig. 5a). The scoring of erythema and edema at the different application sites (Fig. 5b) revealed that **p(b2-PEGDA700)** and **p(b1-PEGDA700)** did not show dermal reactivity.

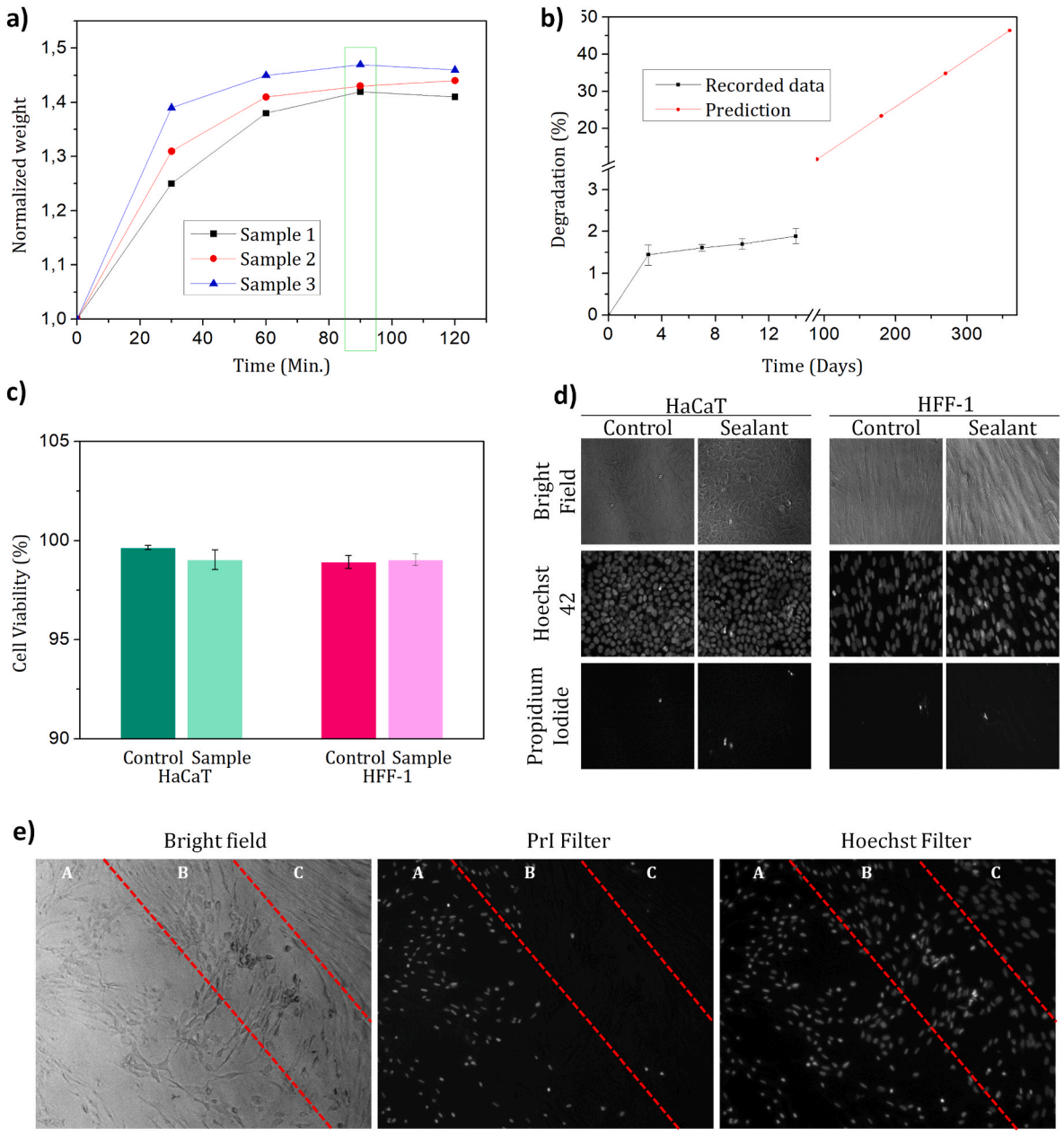

Fig. 4. a) Swelling study of the **p(b2-PEGDA700)** formulation reaching the stability at 90 min. b) Degradation study during 14 days (black). The predicted degradation (red) was calculated considering constant degradation along time.c) Cell viability for HaCaT and HFF-1 cells. d) Representative pictures of HaCaT and HFF-1 cells after 24 h incubation without (control) and with the cured formulation (sealant). H42 dye permeates all cells, whereas PrI only enters cells with compromised membranes, indicating cell death. e) Representative pictures of HFF-1 cells after 24 h incubation with the material cured *in situ* where three regions are differentiated: A) fixed cells with a thin layer of sealant, B) periphery of the cured sealant, and C) farther unaffected fibroblast from the photopolymerized material.

4. Conclusions

In summary, DMS-containing thiolated monomers represent a promising approach for photocurable sealants following a thiol-ene reaction. After exploring different experimental conditions, PEG chains, thiol crosslinking and catechol protection, best results were unexpectedly obtained for the **p(b2-PEGDA700)** formulation, most likely due to a combination of crosslinking capabilities and reaction efficiency. While experimental variability can influence BP, it showed competitive BP values in comparison with existing sealants both in gastrointestinal and external skin applications, but curing under UV light within 60 s and 90 s under the less harmful irradiation with visible light ($\lambda = 430$ nm). Specifically, the obtained values of BP, using blue LED light, are 11.3 ± 0.94 kPa in gastrointestinal pig tissues and 29.6 ± 2.6 kPa in external skin, while Tisseel® and Dermabond® describe 4 kPa and 26 kPa, respectively. The curing time of our material (90 s using 430 nm light) has also to bee hightligted considering the gelation times, between 2 and 5 min, described for Tisseel® and CoSeal® in gastrointestinal tissues. Finally, **p(b2-PEGDA700)** also demonstrated adequate swelling capacity, stability, and degradation performance suited for surgical use, as well as *in vitro* and *in vivo* biocompatibilities. Further work is currently underway to improve the performance of the formulations by analysing and optimizing the experimental parameters and thereby expanding the range of possible applications.

CRediT authorship contribution statement

Alba López-Moral: Writing – review & editing, Writing – original

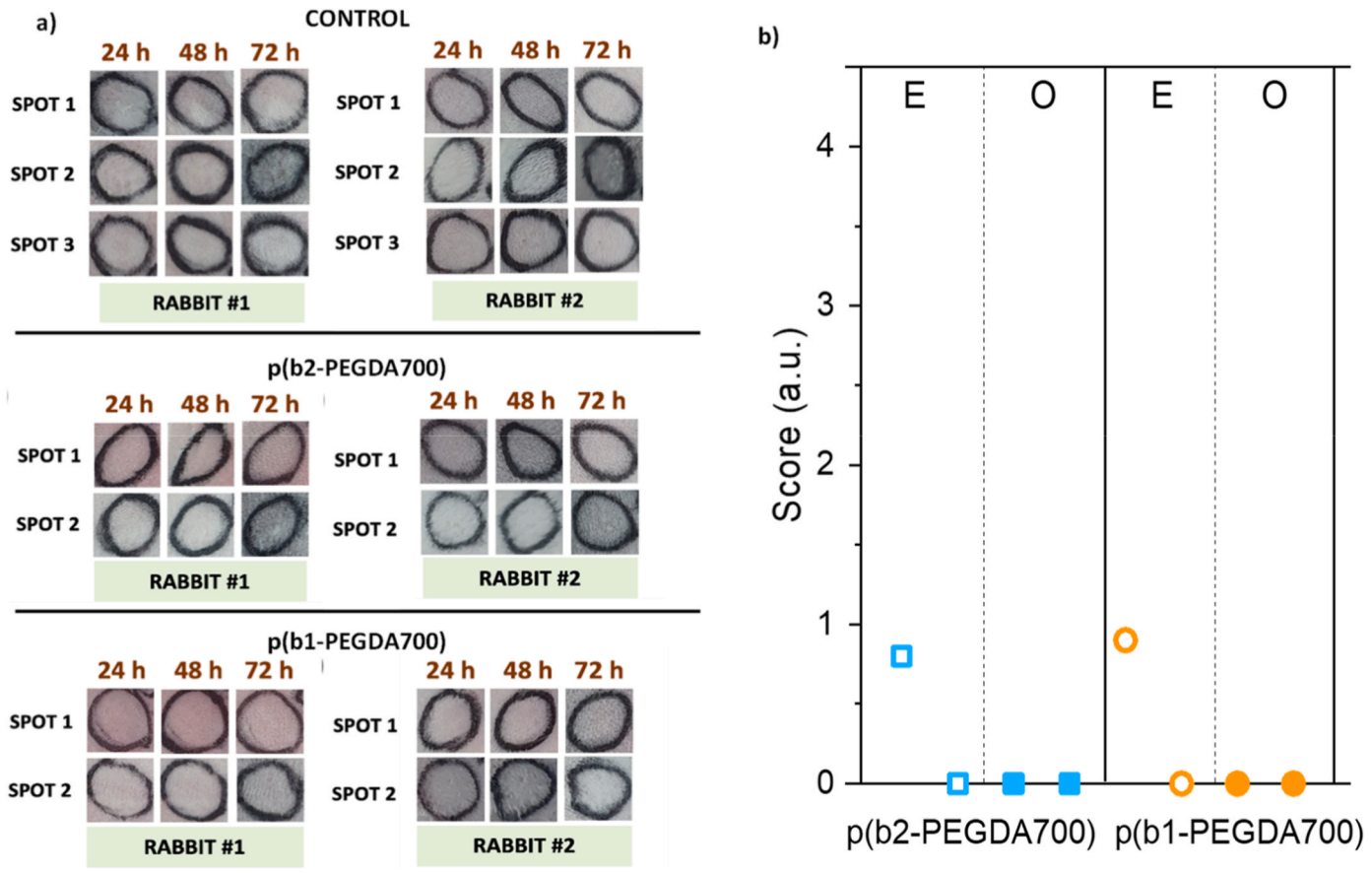

Fig. 5. a) Images of the injection sites of control of physiological saline media, the application of **p(b2-PEGDA700)**, and the application of **p(b1-PEGDA700)**. All injection sites were monitored at 24, 48 and 72 h. b) Results of the scoring of erythema (E) and edema (O) of **p(b2-PEGDA700)** and **p(b1-PEGDA700)** extracts in physiological saline media.

draft, Visualization, Methodology, Investigation, Formal analysis. **Miguel Ángel Moreno-Villaécija:** Writing – review & editing, Validation, Methodology, Investigation, Formal analysis, Data curation, Conceptualization. **Salvio Suárez-García:** Writing – review & editing, Methodology, Formal analysis, Conceptualization. **Jose Bolaños-Cardet:** Writing – review & editing, Methodology, Formal analysis, Data curation. **Josep Sedó-Vegara:** Validation, Supervision, Methodology, Formal analysis, Data curation, Conceptualization. **Ramon Alibés:** Writing – review & editing, Validation, Supervision, Project administration, Methodology, Conceptualization. **Juan Mancebo-Aracil:** Writing – review & editing, Validation, Methodology, Investigation, Conceptualization. **Haritz Sardon:** Writing – review & editing, Validation, Resources, Methodology, Formal analysis. **Haeshin Lee:** Validation, Resources, Data curation. **Claudio Roscini:** Writing – review & editing, Visualization, Validation, Software, Methodology, Formal analysis, Data curation. **Marco Sangermano:** Writing – review & editing, Visualization, Software, Resources, Methodology, Data curation. **Félix Busqué:** Writing – review & editing, Writing – original draft, Visualization, Supervision, Methodology, Investigation, Funding acquisition, Formal analysis, Conceptualization. **Daniel Ruiz-Molina:** Writing – review & editing, Writing – original draft, Validation, Supervision, Resources, Project administration, Methodology, Investigation, Funding acquisition, Data curation, Conceptualization.

Declaration of competing interest

The authors declare that they have no known competing financial interests or personal relationships that could have appeared to influence the work reported in this paper.

Acknowledgments

This work was supported by grants PID2024-161565OB-C21, PID2019-106403RB-I00, and PID2022-139826OB-I00 funded by MICIU/AEI/10.13039/501100011033/and by EUFEDER, and 2021SGR00135. The ICN2 is funded by the CERCA program/Generalitat de Catalunya and supported by the Severo Ochoa Centres of Excellence programme, Grant CEX2021-001214-S, funded by MICIU/AEI/10.13039.50110001103. We acknowledge support of the publication fee by the CSIC Open Access Publication Support Initiative through its Unit of Information Resources for Research (URICI).

Appendix A. Supplementary data

Supplementary data to this article can be found online at https://doi.org/10.1016/j.mtchem.2026.103634.

Data availability

Data will be made available on request.

References

[1] G.M. Taboada, K. Yang, M.J. Pereira, S.S. Liu, Y. Hu, J.M. Karp, N. Artzi, Y. Lee, Overcoming the translational barriers of tissue adhesives, Nat. Rev. Mater. 5 (2020) 310–329, https://doi.org/10.1038/s41578-019-0171-7.
[2] V. Bhagat, M.L. Becker, Degradable adhesives for surgery and tissue engineering, Biomacromolecules 18 (2017) 3009–3039, https://doi.org/10.1021/acs.biomac.7b00969.
[3] Z. Bao, M. Gao, Y. Sun, R. Nian, M. Xian, The recent progress of tissue adhesives in design strategies, adhesive mechanism and applications, Mater. Sci. Eng. C 111 (2020) 1–15, https://doi.org/10.1016/j.msec.2020.110796.

[4] A. Bal-Ozturk, B. Cecen, M. Avci-Adali, S.N. Topkaya, E. Alarcin, G. Yasayan, Y.C. E. Li, B. Bulkurcuoglu, A. Akpek, H. Avci, K. Shi, S.R. Shin, S. Hassan, Tissue adhesives: from research to clinical translation, Nano Today 36 (2021) 1–25, https://doi.org/10.1016/j.nantod.2020.101049.

[5] Z. Ma, G. Bao, J. Li, Multifaceted design and emerging applications of tissue adhesives, Adv. Mater. 33 (2021) 1–29, https://doi.org/10.1002/adma.202007663.

[6] Y. Huang, W. Jing, J. Zeng, Y. Xue, Y. Zhang, X. Yu, P. Wei, B. Zhao, J. Dong, Highly tough and biodegradable Poly(Ethylene Glycol)-Based bioadhesives for arge-scaled liver injury hemostasis and tissue regeneration, Adv. Healthcare Mater. 12 (2023) 2301086, https://doi.org/10.1002/adhm.202301086.

[7] R. Tutar, E. Yüce-Erarslan, B. İzbudak, A. Bal-Öztürk, Photocurable silk fibroin-based tissue sealants with enhanced adhesive properties for the treatment of corneal perforations, J. Mater. Chem. B 10 (2022) 2912–2925, https://doi.org/10.1039/d1tb02502c.

[8] M. Xie, Y. Chen, Q. Yang, Q. Li, R. Zhang, W. Bi, Y.G. Jia, P.K. Chu, H. Wang, X. Shi, Nano-enabled DNA supramolecular sealant for soft tissue surgical applications, Nano Today 50 (2023) 101825, https://doi.org/10.1016/j.nantod.2023.101825.

[9] A. Skardal, S.V. Murphy, K. Crowell, D. Mack, A. Atala, S. Soker, A tunable hydrogel system for long-term release of cell-secreted cytokines and bioprinted in situ wound cell delivery, J. Biomed. Mater. Res., Part B 105 (2017) 1986–2000, https://doi.org/10.1002/jbm.b.33736.

[10] Y. Yongle, Y. Yanyan, Z. Shuxiang, X. Shudan, W. Bingyan, S. Tao, Z. Xin, Y. Shenglian, Z. Haijun, W. Lei, L.-N. Wang, Rapidly photocurable and strongly adhesive hydrogel-based sealant with good procoagulant activity for lethal hemorrhage control, Adv. Funct. Mater. (2025) 2501904, https://doi.org/10.1002/adfm.202501904.

[11] A. Narayanan, Y. Xu, A. Dhinojwala, A. Joy, Advances in photoreactive tissue adhesives derived from natural polymers, ChemEngineering 4 (2020) 32, https://doi.org/10.3390/chemengineering4020032.

[12] H. Ma, Y. Peng, S. Zhang, Y. Zhang, P. Min, Effects and progress of photo-crosslinking hydrogels in wound healing improvement, Gels 8 (2022) 609, https://doi.org/10.3390/gels8100609.

[13] J.R. Yaron, M. Gosangi, S. Pallod, K. Rege, In situ light-activated materials for skin wound healing and repair: a narrative review, Bioeng. Transl. Med. 9 (2024) e10637, https://doi.org/10.1002/btm2.10637.

[14] H. Lee, S.M. Dellatore, W.M. Miller, P.B. Messersmith, Mussel-inspired surface chemistry for multifunctional coatings, Science 318 (2007) 426–430, https://doi.org/10.1126/science.1147241.

[15] C. Zhang, L. Xiang, J. Zhang, C. Liu, Z. Wang, H. Zeng, Z.K. Xu, Revisiting the adhesion mechanism of mussel-inspired chemistry, Chem. Sci. 13 (2022) 1698–1705, https://doi.org/10.1039/d1sc05512g.

[16] F. Liu, X. Liu, F. Chen, Q. Fu, Mussel-inspired chemistry: a promising strategy for natural polysaccharides in biomedical applications, Prog. Polym. Sci. 123 (2021) 101472, https://doi.org/10.1016/j.progpolymsci.2021.101472.

[17] Q. Lin, D. Gourdon, C. Sun, N. Holten-Andersen, T.H. Anderson, J.H. Waite, J. N. Israelachvili, Adhesion mechanisms of the mussel foot proteins Mfp-1 and Mfp-3, Proc. Natl. Acad. Sci. USA 104 (2007) 3782–3786, https://doi.org/10.1073/pnas.0607852104.

[18] Y.K. Jeong, S.H. Park, J.W. Choi, Mussel-inspired coating and adhesion for rechargeable batteries: a review, ACS Appl. Mater. Interfaces 10 (2018) 7562–7573, https://doi.org/10.1021/acsami.7b08495.

[19] (a) C.L. Atencio-Martinez, A. Lancelot, J.J. Wilker, Formulation of catechol-containing adhesives for enhanced underwater bonding and workability, Sci. Technol. Adv. Mater. 26 (2025) 2467617, https://doi.org/10.1080/14686996.2025.2467617;
(b) A.V. Menon, A.A. Putnam-Neeb, C.E. Brown, C.J. Crain, G.J. Breur, S. K. Narayanan, J.J. Wilker, J.C. Liu, Biocompatibility of mussel-inspired water-soluble tissue adhesives, J. Biomed. Mater. Res. 112 (2024) 2243–2256, https://doi.org/10.1002/jbm.a.37775;
(c) R. Xu, S. Ma, P. Lin, B. Yu, F. Zhou, W. Liu, High Strength Astringent Hydrogels Using Protein as the Building Block for Physically Cross-Linked Multi-Network, ACS Appl. Mater. Interfaces 10 (2018) 7593–7601, https://doi.org/10.1021/acsami.7b04290.

[20] J. Bolaños-Cardet, D. Ruiz-Molina, V.J. Yuste, S. Suárez-García, Bioinspired phenol-based coatings for medical fabrics against antimicrobial resistance, Chem. Eng. J. 481 (2024) 148674, https://doi.org/10.1016/j.cej.2024.148674.

[21] H. Montazerian, A.H. Najafabadi, E. Davoodi, R. Seyedmahmoud, R. Haghniaz, A. Baidya, W. Gao, N. Annabi, A. Khademhosseini, P.S. Weiss, Poly-catecholic functionalization of biomolecules for rapid gelation, robust injectable bioadhesion, and near-infrared responsiveness, Adv. Healthcare Mater. 12 (2023) 2203404, https://doi.org/10.1002/adhm.202203404.

[22] M. Ghovvati, S. Baghdasarian, A. Baidya, J. Dhal, N. Annabi, Engineering a highly elastic bioadhesive for sealing soft and dynamic tissues, J. Biomed. Mater. Res. B 110 (2022) 1511–1522, https://doi.org/10.1002/jbm.b.35012.

[23] X. Wu, Z. Wang, J. Xu, L. Yu, M. Qin, J. Li, S. Liu, W. Zheng, Z. Li, J. Ouyang, Y. Li, G. Li, L. Wang, W. Huang, Y. Wu, Photocurable injectable janus hydrogel with minimally invasive delivery for all-in-one treatment of gastric perforations and postoperative adhesions, Theranostics 13 (2023) 5365–5385, https://doi.org/10.7150/thno.87639.

[24] W. Zhang, S. Song, J. Huang, Z. Zhang, An injectable, robust double network adhesive hydrogel for efficient prevention of postoperative tissue adhesion, Chem. Eng. J. 476 (2023) 146244, https://doi.org/10.1016/j.cej.2023.146244.

[25] Q. Wang, X. Zhao, F. Yu, P.-H. Fang, L. Liu, X. Du, W. Li, D. He, Y. Bai, S. Li, J. Yuan, Photocurable and temperature-sensitive bioadhesive hydrogels for suturless sealing of full-thickness corneal wounds, Small Methods 8 (2024) 2300996, https://doi.org/10.1002/smtd.202300996.

[26] C.-Y. Shi, D.-D. He, Q. Zhang, F. Tong, Z.-T. Shi, H. Tian, D.-H. Qu, Robust and dynamic underwater adhesives enabled by catechol-functionalized poly(disulfides) network, Natl. Sci. Rev. 10 (2023) nwac139, https://doi.org/10.1093/nsr/nwac139.

[27] (a) C. Casagualda, A. López-Moral, P. Alfonso-Triguero, J. Lorenzo, R. Alibés, F. Busqué, D. Ruiz-Molina, Biomimetics 9 (2024) 531, https://doi.org/10.3390/biomimetics9090531;
(b) C. Casagualda, J. Mancebo-Aracil, M. Moreno-Villaécija, A. López-Moral, R. Alibés, F. Busqué, D. Ruiz-Molina, Mussel-Inspired Multifunctional Polyethylene Glycol Nanoparticle Interfaces by Mussel-Inspired Lego Approach for Controlling the Wettability of Surfaces with Colorless Coatings, Biomimetics 8 (2023) 3, https://doi.org/10.3390/biomimetics8010003.

[28] C.E. Hoyle, C.N. Bowman, Thiol-ene click chemistry, Angew. Chem. Int. Ed. 49 (2010) 1540–1573, https://doi.org/10.1002/anie.200903924.

[29] A.B. Lowe, Thiol-ene "click" reactions and recent applications in polymer and materials synthesis, Polym. Chem. 1 (2010) 17–36, https://doi.org/10.1039/B9PY00216B.

[30] T.O. Machado, C. Sayer, P.H.H. Araujo, Thiol-ene polymerization: a promising technique to obtain novel biomaterials, Eur. Polym. J. 86 (2017) 200–215, https://doi.org/10.1016/j.eurpolymj.2016.02.025.

[31] D. Ruiz-Molina, J. Sedó, J. Mancebo, Catechol-Derivative Compounds, Polymeric Catechol Compounds and Applications, EP3438093 A1.

[32] C. Bideplán-Moyano, M.J. Lo Fiego, J.J. Calmels, B. Alonso, G. Radivoy, D. Ruiz-Molina, J. Mancebo-Aracil, F. Nador, Design and synthesis of unnatural coordinatin glycopolymer particles (CGPs): unleashing the potential of catechol-saccharide derivatives, RSC Adv. 13 (2023) 27491, https://doi.org/10.1039/D3RA05316D.

[33] M.J. Niedźwiedź, G. Demirci, N. Kantor-Malujdy, M. El Fray, Influence of photoinitiator type and curing conditions on the photocuring of soft polymer network, Materials 16 (2023) 7348–7370, https://doi.org/10.3390/ma16237348.

[34] E. Yoshii, Cytotoxic effects of acrylates and methacrylates: relationships of monomer structures and cytotoxicity, J. Biomed. Mater. Res. 37 (1997) 517–524, https://doi.org/10.1002/(SICI)1097-4636(19971215)37:4%3C517::AID-JBM10%3E3.0.CO;2-5.

[35] R. Holmes, X.-B. Yang, A. Dunne, L. Florea, D. Wood, G. Tronci, Thiol-ene photo-click Collagen-PEG hydrogels: impact of water-soluble photoinitiators on cell viability, gelation kinetics and rheological properties, Polymers 9 (2017) 226, https://doi.org/10.3390/polym9060226.

[36] A. Fritschen, A.K. Bell, I. Königstein, L. Stühn, R.W. Stark, A. Blaeser, Investigation and comparison of resin materials in transparent DLP-printing for application in cell culture and organs-on-a-chip, Biomater. Sci. 10 (2022) 1981–1994, https://doi.org/10.1039/D1BM01794B.

[37] COSEAL. Baxter Home Page. https://advancedsurgery.baxter.com/coseal (accessed October 14, 2025).

[38] TISSEEL. Baxter Home Page.[Product Monograph Template - Schedule D] (accessed October 14, 2025).

[39] R. Karakoyun, U. Gündüz, N. Bülbüller, H. Çalış, M. Habibi, O. Öner, H. Gülkesen, The effects of reinforcement methods on burst pressure in resected sleeve gastrectomy specimens, J. Laparoendosc. Adv. Surg. Tech. 25 (2015) 64–68, https://doi.org/10.1089/lap.2014.0408.

[40] DERMABOND ADVANCED ™ and mini topical skin adhesive. Johnson&Johnson MedTech Home page. https://www.jnjmedtech.com/en-US/product/dermabond-advanced-mini-topical-skin-adhesives (accessed October 14, 2025).

[41] A. Ashrafi, E. Khadem, M. Kharaziha, Engineering a mussel-inspired hemostatic sealant with a strong tissue anchor as a first-aid tissue adhesive, Mater. Today Chem. 35 (2024) 101864–101880, https://doi.org/10.1016/j.mtchem.2023.101864.

[42] G. Schultz, G. Chin, L. Moldaver, R. Diegelmann, Principes of wound healing (chapter 23) in: Mechanisms of Vascular Disease, Barr Smith Press, University of Adelaida Presss. ISBN (paperback) 978-0-9871718-2-5 Bookshelf_NBK534260.pdf.

[43] S. Singh, A. Young, C.-E. McNaught, The physiology of wound healing, Surgery 35 (2017) 473–477, https://doi.org/10.1016/j.mpsur.2017.06.004.

[44] M.V. Plikus, X. Wang, S. Sinha, E. Forte, S.M. Thompson, E.L. Herzog, R.R. Driskell, N. Rosenthal, J. Biernaskie, V. Horsley, Fibroblast: origins, definitions, and functions in health and disease, Cell 184 (2021) 3852–3872, https://doi.org/10.1016/j.cell.2021.06.024.

[45] M.S. Al-Dhubaibi, G.F. Mohammed, S.S. Bahaj, A.I. AbdElneam, A.M. Al-Dhubaibi, L.M. Atef, The role of keratinocytes in skin health and disease, Dermatological Reviews 6 (2025) e70028, https://doi.org/10.1002/der2.70028.